

Lifetimes of the $9s$ and $8p$ levels of atomic francium

S. Aubin,* E. Gomez, L. A. Orozco,[†] and G. D. Sprouse

Department of Physics and Astronomy, State University of New York, Stony Brook, New York 11794-3800, USA

(Received 10 May 2004; published 20 October 2004)

We use time-correlated single-photon counting techniques on a sample of ^{210}Fr atoms confined and cooled in a magneto-optical trap to measure the lifetimes of the $9S_{1/2}$, $8P_{3/2}$, and $8P_{1/2}$ excited levels. We populate the $9S_{1/2}$ level by two-photon resonant excitation through the $7P_{1/2}$ level. The direct measurement of the $9S_{1/2}$ decay through the $7P_{3/2}$ level at 851 nm gives a lifetime of 107.53 ± 0.90 ns. We observe the decay of the $9S_{1/2}$ level through the $8P_{3/2}$ level at 423 nm and the $8P_{1/2}$ level at 433 nm down to the $7S_{1/2}$ ground level, and indirectly determine the lifetimes of these to be 83.5 ± 1.5 ns and 149.3 ± 3.5 ns, respectively.

DOI: 10.1103/PhysRevA.70.042504

PACS number(s): 32.70.Cs, 32.80.Pj, 32.10.Dk

I. INTRODUCTION

A precise understanding of the electronic wave functions of the excited levels of francium is important for the analysis of measurements of parity nonconservation (PNC) in this element [1–3]. The potential use of this element in PNC measurements is tied to the simplicity of its alkali atomic structure and large parity mixing [4,5]. Since atomic PNC measurements probe the mixing of s and p wave functions, these must be well understood to accurately extract parameters and constraints on the electroweak force of the standard model.

We present here our measurements of the lifetimes of the $9s$, $8P_{3/2}$, and $8P_{1/2}$ levels. These three spectroscopic measurements test the accuracy of the wave functions of the francium valence electron for both the ground and excited levels, and probe the behavior of the wave functions at large electronic radii. We have performed similar measurements on the $7s$ and $6p$ levels of ^{85}Rb , where the average number of trapped atoms is larger, to search for systematic errors [6].

The production, cooling and trapping of francium on-line with the Superconducting LINAC at Stony Brook has been described previously [7]. Briefly, we produce francium in a nuclear fusion reaction between a gold target and a 100 MeV $^{18}\text{O}^{+5}$ beam from the Stony Brook superconducting LINAC. With $\sim 1 \times 10^6$ $^{210}\text{Fr}^+$ /s extracted from the target and transported to the trapping region, we cool and trap 10^4 – 10^5 atoms in steady state with our pulsed high efficiency MOT.

Figure 1 shows the energy levels of ^{210}Fr relevant for cooling, trapping, and the lifetime measurements. A Coherent 899-21 titanium-sapphire (Ti:sapphire) laser operating at 718 nm excites the trapping and cooling transition ($7S_{1/2}, F=13/2 \rightarrow 7P_{3/2}, F=15/2$). A Coherent 899-01 Ti:sapphire laser operating at 817 nm repumps atoms that leak out of the cooling cycle via the $7S_{1/2}, F=11/2 \rightarrow 7P_{1/2}, F=11/2$ transition. A second Coherent 899-21 Ti:sapphire laser operating at 744 nm excites the francium atoms to the $9s$ level through

the $7P_{1/2} \rightarrow 9S_{1/2}$ transition. We measure lifetimes of the atom by abruptly turning off the excitation and observing the time dependence of the subsequent decays of fluorescence. An atom excited to the $9s$ level returns indirectly to the ground level through several decay channels. The $9s$ level decays to the $8p$ and $7p$ levels. While both of these levels decay directly to the $7s$ ground level, the $8p$ levels also decay to the $8s$ and $6d$ levels, which then decay to the ground level through the $7p$ levels. We measure the lifetime of the $9s$ level through its decay to the $7P_{3/2}$ level. We obtain the $8P_{3/2}$ and $8P_{1/2}$ lifetimes through the decay of these levels to the $7s$ level. Figure 2 shows the three decay transitions relevant to the lifetime measurements.

This paper is divided into four parts. Section II explains the apparatus and method used for measuring the lifetimes, Sec. III presents the measurement of the $9S_{1/2}$ lifetime, Sec. IV details the measurements of the $8P_{3/2}$ and $8P_{1/2}$ lifetimes, and Sec. V concludes.

II. METHOD AND APPARATUS

A. Method: time-correlated single-photon counting

We measure the lifetimes using time-correlated single-photon counting [8]. This method has been used, for example, to measure lifetimes of atoms in beams [9], atoms in

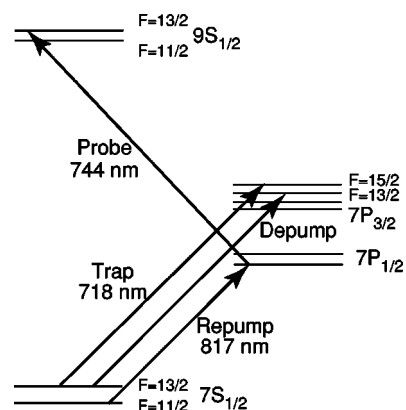


FIG. 1. ^{210}Fr energy levels and lasers relevant to the trap operation and excitation of the $9S_{1/2}$ level.

*Present address: Department of Physics, University of Toronto, Toronto, Ontario, Canada, M5S 1A7.

[†]Present address: Department of Physics, University of Maryland, College Park, MD 20742, USA.

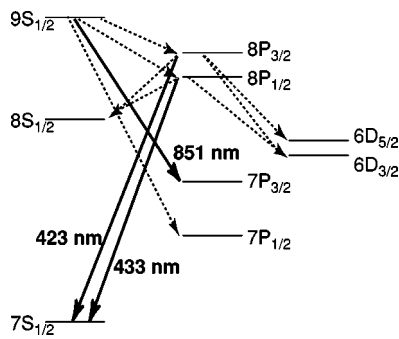


FIG. 2. Energy levels and decay channels of ^{210}Fr involved in the decays of the $9s$ and $8p$ levels. The observed decay transitions relevant to the measurements of the $9S_{1/2}$, $8P_{3/2}$, and $8P_{1/2}$ lifetimes are indicated by full line arrows and the wavelength of the emitted photon. The unobserved decay transitions are represented by dashed line arrows.

vapor cells [10], and trapped single ions [11]. The Francium Spectroscopy Group at Stony Brook has used the technique for the lifetime measurements of the $7p$ and $7d$ levels of trapped atomic francium [12,13]. This section describes in greater detail the method used for the previously published $9s$ lifetime [14].

The time-correlated single-photon counting technique uses a short pulse of resonant laser light to populate an excited state at $t=0$. When the atoms decay from their excited state to a lower lying state they emit a photon. The arrival times at the photodetector, with respect to the excitation pulse, of the spontaneously emitted photons are distributed according to the exponential decay of the state. The lifetime of the state is extracted from an exponential fit to the histogram of the arrival times.

B. Apparatus

Figure 3 shows the basic elements of the apparatus. We pulse the excitation laser at 744 nm with two Gsänger LM0202 electro-optic modulators (EOM) and one Crystal Technologies acousto-optic modulator (AOM). The three modulators in series allow us to turn off the excitation laser with an extinction ratio better than 400:1 in less than 20 ns. Figure 4 shows the turn off the 744 nm excitation laser as measured with a photomultiplier tube (Hamamatsu R636)

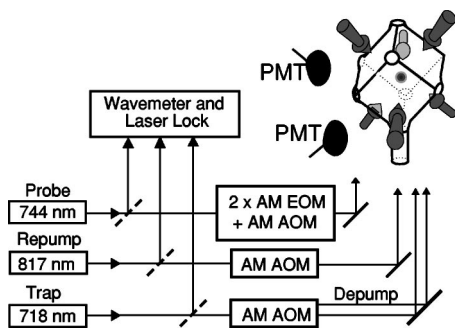


FIG. 3. Block diagram of $9s$ and $8p$ spectroscopy experiment.

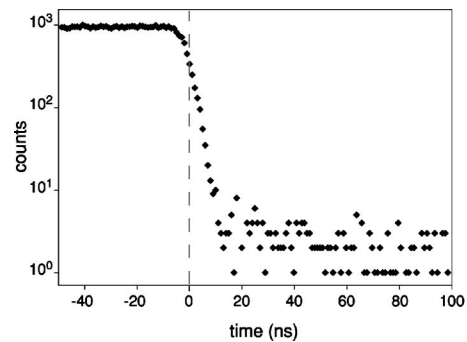


FIG. 4. Turn off the 744 nm excitation laser as measured with the time-correlated single photon counting detection electronics. No dark count background has been subtracted. $t=0$ corresponds to the time at which the probe laser has fallen to $1/e$ of its on amplitude. The data were accumulated over 5×10^7 cycles (500 s).

and the time correlated single-photon counting electronics.

To minimize background, we excite from the $7P_{1/2}$ state at 744 nm. We move population to the $7S_{1/2}, F=11/2$ state with a depumping laser ($7S_{1/2}, F=13/2 \rightarrow 7P_{3/2}, F=13/2$) that puts atoms into the $7S_{1/2}, F=11/2$ state where the repumper can take them to the $7P_{1/2}, F=11/2$ state (see Fig. 3). A Burleigh WA-1500 wavemeter monitors the wavelength of the lasers to about $\pm 0.001 \text{ cm}^{-1}$, while a computer-controlled scanning Fabry-Pérot cavity monitors and holds the long-term frequencies of all lasers at the MHz level [15]. A charge-coupled-device (CCD) camera collects the trapping cycle fluorescence and monitors the number of atoms in the trap during measurements. We operate in a regime where the steady-state number of atoms is small, roughly 10^4 , to make sure that the density of the sample is low (trap diameter $\approx 0.2 \text{ mm}$).

The measurement operates on a $10 \mu\text{s}$ cycle sketched in Fig. 5. We excite a fraction of the atoms in the $7P_{1/2}$ state with the 744 nm probe laser. Following the probe pulse, we detect the decay of fluorescence back to the $7P_{3/2}$ state at 851 nm for $1.3 \mu\text{s}$. We cool and trap the atoms during the rest of the cycle. All lasers are turned on and off at the appropriate times to optimize the measurement of the excited state lifetime.

When the PMT detects a photon, it generates a variable amplitude electronic pulse. We first amplify the signal with an Ortec AN106/N linear amplifier and then send it to an Ortec 934 constant fraction discriminator (CFD). The CFD outputs a sharp constant height pulse triggered on a constant fraction of the amplitude of the input pulse. The delay of the

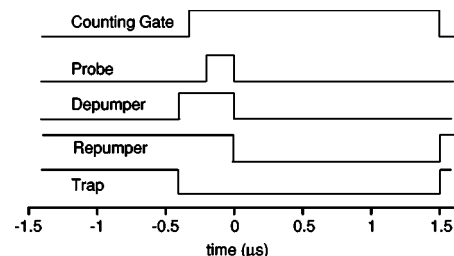


FIG. 5. Timing diagram for $9s$ lifetime measurement.

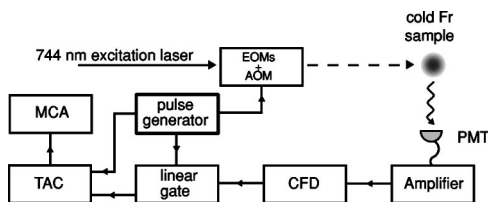


FIG. 6. Block diagram of electronics used for processing a photon detection pulse.

output pulse with respect to the input pulse is independent of the amplitude of the input pulse. The output of the CFD is sent to an Ortec LG101/N linear gate to eliminate photon pulses detected before the excitation pulse. The output of the linear gate is sent to the start input of an Ortec 467 time-to-amplitude converter (TAC). We send a stop pulse generated by the master clock to the stop input of the TAC 2.8 μ s after the excitation laser pulse is applied. Starting the TAC with a fluorescence photon eliminates the accumulation of counts from cycles with no detected photons. A multichannel analyzer (MCA) bins the TAC output to produce a histogram of the events. We use an EG&G Ortec Trump-8k MCA for the $9s$ lifetime measurement and a Canberra 3502 MCA for the $8p$ lifetime measurements. A Berkeley Nucleonics Corporation BNC 8010 pulse generator and two Stanford Research Systems DG535 pulse delay generators provide the timing sequence for the chopping of lasers, the linear gate, and the TAC stop pulse. Figure 6 is a block diagram of the detection pulse electronics.

A 1:1 imaging system ($f/3.9$) collects the fluorescence onto both a high-speed cooled CCD camera (Roper Scientific, MicroMax 1300YHS-DIF) for the trapping light at 718 nm and a Hamamatsu R636 photomultiplier tube (PMT) for the lifetime measurement at 851 nm. An Andover 851 nm (10 nm FWHM passband) filter in front of the PMT reduces spurious photon counts from 718 nm, 817 nm, 744 nm, and background room light. A second 1:1 imaging system ($f/3.9$) directs fluorescence from the decay of the $8p$ levels to the ground level at 423 nm and 433 nm (see Fig. 2) onto an Amperex XP2020(Q) PMT. The photon counting electronics are similar to those used for counting the 851 nm photons, though we use a different MCA for the $8p$ lifetime measurements. We collect the data for the $8p$ lifetime measurements in parallel with the $9s$ lifetime data. We keep the rate of photon counts low to prevent double pulse events and reduce dead-time systematic effects in the electronics.

The two Gsänger LM0202 EOMs produce large voltage spikes and associated radio-frequency (rf) noise when they chop the 744 nm excitation laser. The rf broadcast from the EOMs is quite large and can have a significant effect on the detection pulse electronics. We reduce the influence of the EOMs to negligible levels by placing them and their associated drivers in an adjoining room and installing them inside a metal mesh cage.

III. LIFETIME OF THE $9s$ LEVEL

We accumulate data for periods of about 1000 seconds with atoms in the trap and the probe laser on resonance. The

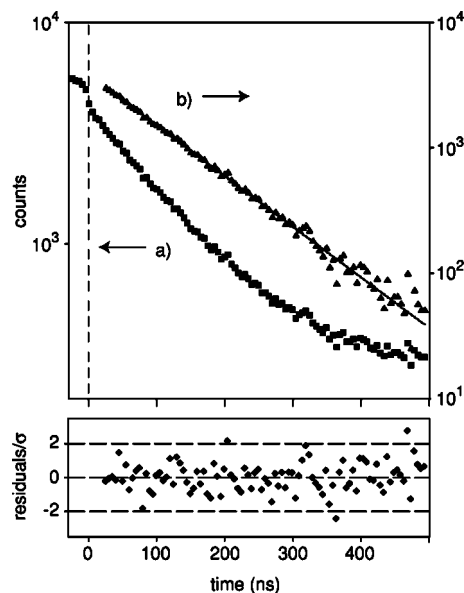


FIG. 7. Decay curve of the $9S_{1/2}$ level with fit residuals. The upper plot displays (a) the original arrival time histogram data, and (b) the same data minus a background with a fit to an exponential decay (solid line). The lower plot shows the residuals of the fit divided by the statistical uncertainty of each point. The data is the sum of several data sets and corresponds to an accumulation time of over 6600 s.

individual data sets are then processed, added together, and fitted. We repeat the counting measurement without atoms and obtain a background.

1. Fit of data

We fit the combined data to a decaying exponential plus a linear background. We use the function

$$N = A \exp(-t/\tau) + b + mt, \quad (1)$$

where τ is the lifetime of the $9s$ level, A is the amplitude of the exponential decay at $t=0$, and b and m describe a linear background. We start the fits 25 ns after the excitation laser turn off to avoid contaminating fits with spurious background from the imperfect turn off of the repumper, depumper, and excitation lasers. The fitting function describes the data well, and we obtain $\chi^2_\nu = 1.00 \pm 0.02$ over several data sets. Figure 7 shows data from the $9s$ lifetime measurement for a 200 ns excitation, a fit to the data minus the background, and the normalized residuals for the fit. We find a linear background with a slope of 2 counts per 1000 channels for 1000 seconds of counting. While the linear background is small, it influences the fits. The background comes from slow turn off of the trap laser with a high efficiency single-pass AOM. The trap laser is focused to a line instead of a point as it passes through the AOM for higher diffraction efficiency but slower turn off time. The trapping laser (at 718 nm) is the strongest, and despite the interference filter, some of the trapping light reaches the PMT.

A. Systematic errors

We have studied the contribution of several sources of systematic errors which can influence the $9s$ lifetime mea-

TABLE I. Error budget for the $9s$ lifetime measurement.

Error	$9S_{1/2}$ (%)
Statistical	± 0.72
Time calibration	$< \pm 0.01$
TAC/MCA nonlinearity	± 0.04
Quantum beats	$< \pm 0.2$
Trap displacement from ^{85}Rb tests	$< \pm 0.38$
Total	$\pm 0.84\%$

surement. We have quantified the contribution of the TAC and MCA nonlinearity, pulse pileup, truncation error, and quantum beats.

(a) *TAC and MCA nonlinearity.* We calibrate the timing of the pulse detection by sending a series of start and stop pulses of known delays from the DG535 pulse generators to the TAC, and record the resulting spectrum on the MCA. We determine the linear time calibration of the TAC and MCA with an uncertainty of $\pm 0.005\%$. The time scale has a small nonlinearity, which adds an uncertainty of $\pm 0.04\%$ to the lifetime of the fitted data. We measure the uniformity of the height scale of the TAC and MCA by taking data with no atoms and no lasers, with room light providing a source of random photons. We find a deviation from flat of 0.09% over 1000 channels. The nonuniformity affects the fitted lifetime by less than 0.01% .

(b) *Pulse pileup correction.* For a given cycle the TAC can only register one photon. A correction to the raw data accounts for the preferential counting of early events [8]. If N_i is the number of counts in MCA channel i , and n_E is the total number of excitation cycles, then N'_i the corrected number of counts in channel i is given by

$$N'_i = \frac{N_i}{1 - \frac{1}{n_E \sum_{j<i} N_j}}. \quad (2)$$

Low count rates, less than one count every 400 cycles, keep this correction small. The correction alters the fitted lifetime of our combined data by less than 0.01% .

(c) *Truncation error.* We find a variation in the fitted lifetime depending on the beginning and ending of the data range we use for the fitting. The truncation error is the standard deviation of the lifetime for different starting and ending points of the fit. We conclude that varying the start and end points of the data set does not lead to statistically significant changes in the fitted lifetime. Fits of artificial data from a Monte Carlo simulation of exponential counts on a linear background show comparable variations that are not statistically significant.

(d) *Quantum beats.* We have searched for quantum beats in the fluorescence decay signal but have not observed any. Since we operate in a MOT, we cannot turn off the magnetic field fast enough for the measurements. Instead, we measure the lifetime as a function of the magnetic gradient, but find no significant trend. We also adapt previous calcu-

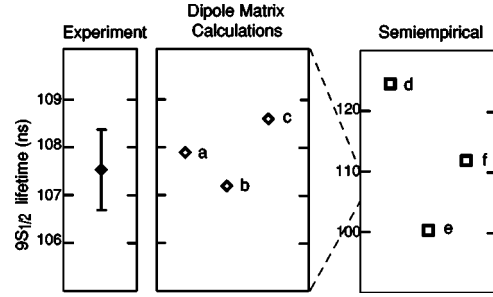


FIG. 8. Comparison of the measured $9S_{1/2}$ level lifetime with theoretical predictions from radial matrix elements (a) [16], (b) [17], (c) [18], and semiempirical calculations (d) [20], (e) [21], (f) [22]. This figure corrects some numbers from Fig. 4 of a previous article [14].

lations for the expected quantum beat signal [12,13] to put an upper limit of $\pm 0.2\%$ in the error budget.

(e) *Other systematic effects.* The density of the atoms in the trap is low ($\sim 10^9/\text{cm}^3$). In this regime, effects such as radiation trapping, superfluorescence, and quenching due to collisions do not alter the measured lifetime. We have carried out with the same apparatus measurements of the lifetime of the $7s$ level of ^{85}Rb [6] and found a systematic error in the lifetime due to a displacement of the trap center. We observe that an imbalance of the trap laser beams due to attenuation of the retroreflected trapping beams displaces the trap center by one trap diameter (~ 0.2 mm) and affects the measured lifetime by $\pm 0.38\%$. This systematic error is below the statistical resolution of the $9s$ measurement in ^{210}Fr , but we include it in the error budget.

B. Summary of measurement

Table I contains the error budget for the lifetime measurements. The measurement is dominated by the statistical error and to a lesser extent by the trap displacement error. Combining the uncertainties in quadrature gives a total uncertainty of $\pm 0.84\%$. We obtain a lifetime of 107.53 ± 0.90 ns for the $9s$ level of ^{210}Fr .

C. Comparison with theory

Figure 8 compares our lifetime measurement results with theoretical predictions. The $9S_{1/2}$ level can decay to the $7P_J$ and $8P_J$ levels ($J=1/2, 3/2$). We use the appropriate reduced radial matrix elements from *ab initio* MBPT theory [16,17], or a one-active electron potential [18] using our measured energies [19] to carry out the calculation of the lifetime [13]. The figure also shows semiempirical calculations of the lifetime [20–22].

The lifetime τ_i of an excited state $|i\rangle$ is determined by its individual decay rates, $\tau_{i \rightarrow j}$, to other states $|j\rangle$ by

$$\frac{1}{\tau_i} = \sum_j \frac{1}{\tau_{i \rightarrow j}}. \quad (3)$$

The decay rates $\tau_{i \rightarrow j}$ are related to the reduced matrix element between states $|i\rangle$ and $|j\rangle$ by

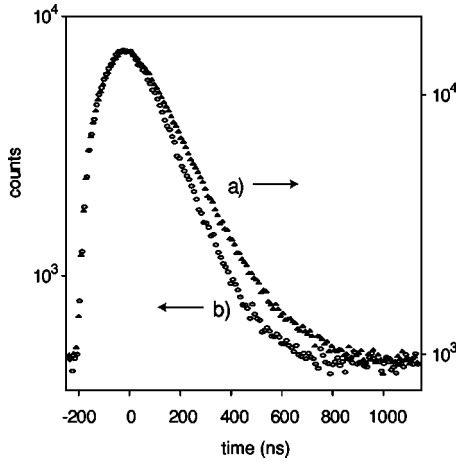


FIG. 9. Photomultiplier tube counts with (a) 436 nm (circles) and (b) 420 nm (triangles) filters—note that the two log scales are the same, but differ by an offset.

$$\frac{1}{\tau_{i \rightarrow j}} = \frac{4}{3} \frac{\omega_{ij}^3}{c^2} \alpha \frac{|\langle J_i || r || J_j \rangle|^2}{2J_i + 1}, \quad (4)$$

where ω_{ij} is the transition frequency in radians/s, c is the speed of light, α is the fine structure constant, J_i and J_j are the respective angular momenta of states $|i\rangle$ and $|j\rangle$, and $\langle J_i || r || J_j \rangle$ is the reduced matrix element of the decay channel.

The calculations from the radial matrix elements make predictions within our experimental uncertainty. The *ab initio* calculations of Safronova *et al.* [16], and Dzuba *et al.* [17] are impressive given the complexity of the atom where large correlation contributions add with opposite sign. The prediction of Marinescu *et al.* [18] is also very good and serves as a quantitative test for their work on van der Waals coefficients for francium.

IV. LIFETIMES OF THE $8p$ LEVELS

We follow the experimental method used for the $9s$ level to measure the lifetimes of the $8P_J$ levels ($J=1/2, 3/2$). We use a 420 nm filter (10 nm FWHM passband, Andover) or a 436 nm filter (5 nm FWHM passband, Andover) in front of the PMT to select primarily photons from the decay of the $8P_{3/2}$ level or the $8P_{1/2}$ level, respectively. Figure 9 shows the different recorded decays with the 420 nm and 436 nm filters. The variation in the decay of the fluorescence with the two filters indicates a significant difference in the lifetimes of the $8P_{3/2}$ and $8P_{1/2}$ levels. The method we employ for measuring the $8P_J$ ($J=1/2, 3/2$) lifetimes of francium is similar to that used in cesium for the $5D_{5/2}$ level [10] and in ytterbium [23].

A. Decay model

The extraction of the $8P_{3/2}$ and $8P_{1/2}$ lifetimes differs significantly from that of the $9s$ lifetime and follows a different decay model. The recorded fluorescence decay at 423 nm and 433 nm depends on the lifetimes of both the $9s$ level and the relevant $8p$ level. For conciseness, 1 refers to the $9s$

level, 2 to the $8P_{3/2}$ level, and 3 to the $8P_{1/2}$ level.

An $8p$ level (either $8P_{3/2}$ or $8P_{1/2}$) is populated through the decay of the $9S_{1/2}$ level. Atoms in the $8P_i$ level are generated at a rate of $\gamma_{1 \rightarrow i} / \tau_1$ per atom in the $9S_{1/2}$ level, where $\gamma_{1 \rightarrow i}$ is the branching ratio of the $9S_{1/2}$ level to the $8P_i$ level. Atoms in the $8P_i$ level are depleted at a rate of τ_i^{-1} per atom, where τ_i is the lifetime of the $8P_i$ level. The rate equation for the population in the $8P_i$ level is given by

$$\frac{d}{dt} p_i = -\frac{1}{\tau_i} p_i + \frac{\gamma_{1 \rightarrow i}}{\tau_1} p_1, \quad (5)$$

where p_1 and p_i are the atomic populations in the $9S_{1/2}$ and $8P_i$ levels, respectively. The solution to this differential equation is

$$p_i(t) = A_i \exp(-t/\tau_1) + B_i \exp(-t/\tau_i), \quad (6)$$

where $\tau_1 = 107.53 \pm 0.90$ ns is the lifetime of the $9s$ level, and A_i and B_i are the amplitudes at $t=0$ of the exponential decays with time constants τ_1 and τ_i , respectively. If the atomic populations reach a steady state during the excitation, and the excitation is turned off at $t=0$, then

$$A_i = \frac{\tau_i}{\tau_1 - \tau_i} N_1 \gamma_{1 \rightarrow i}, \quad B_i = \left(\frac{\tau_i}{\tau_1} - \frac{\tau_i}{\tau_1 - \tau_i} \right) N_1 \gamma_{1 \rightarrow i}. \quad (7)$$

where N_1 is the number of atoms in the $9s$ level at $t=0$.

B. Fitting procedure

In practice, despite the use of interference filters, the photons from the decay of the $8P_{3/2}$ and $8P_{1/2}$ levels cannot be completely isolated from one another. Inevitably, photon counts recorded with the 420 nm filter include a small fraction of counts due to 433 nm photons. Similarly, the data taken with the 436 nm interference are contaminated by counts due to 423 nm photons.

The contamination photons must be accounted for to correctly extract the $8P_{3/2}$ and $8P_{1/2}$ lifetimes from the data. More specifically, the fitting function must include the decays of both levels. Since the photon emission rate is equal to the atom loss rate p_i / τ_i , the PMT registers dN_{PMT} photon counts in an infinitesimal time dt according to the following equation:

$$dN_{\text{PMT}}(t) = \{ \beta [\gamma_{2 \rightarrow 7s} T(\lambda_2) \tau_2^{-1} p_2(t) + \gamma_{3 \rightarrow 7s} T(\lambda_3) \tau_3^{-1} p_3(t)] + b \} dt, \quad (8)$$

where β is the probability to detect an emitted photon, and $\gamma_{2 \rightarrow 7s}$ and $\gamma_{3 \rightarrow 7s}$ are the branching ratios to the $7s$ level of the $8P_{3/2}$ and $8P_{1/2}$ levels, respectively. $T(\lambda)$ is the transmission of the filter in use as a function of the wavelength λ , and $p_2(t)$ and $p_3(t)$ are given by Eq. (6).

From the data we have $N_{\text{PMT}}(t)$ from which we must extract the parameters of the functions $p_i(t)$ for $i=2,3$. We construct the fitting function by absorbing all constants and coefficients into the exponential amplitudes. According to Eq. (8) the data recorded as $N_{\text{PMT}}(t)$ over a time interval δt (bin size of MCA histogram) is described by the following fitting function for $\delta t \ll \tau_i, \tau_1$

$$N_{\text{PMT}}(t) = C_2 P_2(t) + C_3 P_3(t) + b, \quad (9)$$

where C_2 and C_3 are the respective amplitudes of the decays through the $8P_{3/2}$ and $8P_{1/2}$ levels, given by $P_2(t)$ and $P_3(t)$ which we define as ($t \geq 0$)

$$P_i(t) = (A_i/B_i) \exp(-t/\tau_i) + \exp(-t/\tau_i). \quad (10)$$

In practice, due to the use of the interference filters, we take data such that the number of counts due to one of the two $8p$ levels is much larger, denoted $i=l$, than the other, denoted $i=s$. The interference filters guarantee that $C_l \gg C_s$. In such data, the signal-to-noise is not sufficient to extract C_l , A_l/B_l , τ_l , C_s , A_s/B_s , τ_s , and b simultaneously and reliably. We resolve this difficulty by treating the smaller term, $C_s P_s(t)$, as a perturbation: If we estimate $C_s P_s(t)$ from other data, then we can extract the parameters of the term, $C_l P_l(t)$, much more precisely from a fit to the data. The method reduces the fitting function given by Eq. (9) from seven parameters to four independent parameters.

We determine the smaller term, $C_s P_s(t)$, in a two step process. (1) We extract an initial estimate of the functional form of $P_i(t)$, given by A_i/B_i and the lifetime τ_i , from fits to data in which the counts due to the $8P_i$ level dominate those from the other level; we do this for both levels. (2) We estimate the relative strength of $C_s P_s(t)$ by measuring the ratio of total $8P_l$ photons counts to total $8P_s$ photon counts, which obeys the following relation:

$$\frac{(\text{Total counts due to } \lambda_l \text{ photons})}{(\text{Total counts due to } \lambda_s \text{ photons})} = \frac{\int C_l P_l(t) dt}{\int C_s P_s(t) dt} \quad (11)$$

$$= \frac{T(\lambda_l) \gamma_{1 \rightarrow l} \gamma_{l \rightarrow 7s}}{T(\lambda_s) \gamma_{1 \rightarrow s} \gamma_{s \rightarrow 7s}}, \quad (12)$$

where the integrals are taken from the start of the excitation until the effective end of the decay. If $T(\lambda_l)/T(\lambda_s)$, $(\gamma_{1 \rightarrow l} \gamma_{l \rightarrow 7s})/(\gamma_{1 \rightarrow s} \gamma_{s \rightarrow 7s})$, $P_l(t)$, and $P_s(t)$ are known then C_l/C_s can be estimated with Eqs. (11) and (12). The data taken with $C_l \gg C_s$ can then be fitted again with the fitting function of Eq. (9), but with A_l/B_l , τ_l , C_l , and b as free parameters and A_s/B_s , τ_s , and C_s/C_l held constant.

We measure $T(\lambda)$ of the interference filters at normal incidence with a CARY 1 UV-Visible spectrometer. For the 420 nm filter, we find $T(423 \text{ nm})/T(433 \text{ nm}) = 242 \pm 27$. For the 436 nm filter, we obtain $T(433 \text{ nm})/T(423 \text{ nm}) = 184 \pm 55$. The error on these two ratios is dominated by the uncertainty in determining the interference filter performance when used in the imaging system. We determine $(\gamma_{1 \rightarrow l} \gamma_{l \rightarrow 7s})/(\gamma_{1 \rightarrow s} \gamma_{s \rightarrow 7s})$ using two methods:

(a) We determine $(\gamma_{1 \rightarrow l} \gamma_{l \rightarrow 7s})/(\gamma_{1 \rightarrow s} \gamma_{s \rightarrow 7s})$ with a broadband filter which has a similar transmission at both 423 nm and 433 nm [$T(423 \text{ nm})/T(433 \text{ nm}) = 1.16 \pm 0.03$]. In this case, we have data with $C_2 \sim C_3$. In order to use Eqs. (11) and (12), we must perform the integrals from the start of the excitation to the end of the decay. We extend $P_i(t)$ defined in Eq. (10) to include piecewise the excitation empirically: the

excitation fitting function is continuous with the decay function of Eq. (10), and its parameters for the $8P_{3/2}$ and $8P_{1/2}$ levels are determined by fitting the excitation data taken with the 420 nm and 436 nm filters, respectively. The exact form of the fitting function is unimportant so long as it describes the excitation data well, since it is only necessary for determining the area under the curve. We fit the broadband filter data with Eq. (9) and the piecewise extended version of $P_i(t)$, but with only C_2 , C_3 , and b as free parameters of the fit, while keeping A_2/B_2 , τ_2 , A_3/B_3 , τ_3 , and the excitation parameters constant at their previously determined values (initial estimates). In this manner, we obtain $[\int C_l P_l(t) dt]/[\int C_s P_s(t) dt]$, from which we extract $(\gamma_{1 \rightarrow l} \gamma_{l \rightarrow 7s})/(\gamma_{1 \rightarrow s} \gamma_{s \rightarrow 7s})$.

(b) Alternatively, we use a second method to determine $(\gamma_{1 \rightarrow l} \gamma_{l \rightarrow 7s})/(\gamma_{1 \rightarrow s} \gamma_{s \rightarrow 7s})$ from the ratio of the average photon count rates obtained with the two interference filters under similar experimental conditions. By taking into account the transmission of the interference filters with Eq. (12), we find $(\gamma_{1 \rightarrow l} \gamma_{l \rightarrow 7s})/(\gamma_{1 \rightarrow s} \gamma_{s \rightarrow 7s})$. The contamination due to unwanted photons is small and does not affect the ratio significantly. This second approach is limited primarily by variations in the laser power and trap population over the course of the measurement.

The combined result with both approaches gives the ratio $(\gamma_{1 \rightarrow 2} \gamma_{2 \rightarrow 7s})/(\gamma_{1 \rightarrow 3} \gamma_{3 \rightarrow 7s}) = 4.7 \pm 1.3$. Theoretical predictions based on electric dipole matrix elements are in agreement with this measurement: The dipole matrix elements of Saffronova *et al.* [16] give a ratio of 3.45, while those of Dzuba *et al.* [24] give a ratio of 4.60. When only fitting the data which is collected after the excitation laser is turned off, then a correction to this ratio is obtained by calculating the integrals in Eq. (11) over only the corresponding time range of the data. Equations (11) and (12) can be used thus to extract an estimate for C_l/C_s and consequently fix the $C_s P_s(t)$ term in Eq. (9).

The procedure for determining $C_s P_s(t)$ is inherently recursive, since it requires knowledge of the parameters of $P_s(t)$, which we are trying to determine. The method functions and converges to stable parameter values, because the initial knowledge of the parameters obtained in step 1 is already quite accurate, due to the high extinction of unwanted photons by the interference filters. We iterate through the procedure twice in order to verify that our uncertainty in $(\gamma_{1 \rightarrow l} \gamma_{l \rightarrow 7s})/(\gamma_{1 \rightarrow s} \gamma_{s \rightarrow 7s})$ is limited by the statistics of the broadband filter data. We define the *contamination shift* $\delta\tau_i$ of a lifetime τ_i to be the difference in lifetimes obtained by including the λ_s photons and neglecting them in the fits of the data. For our data, the contamination shifts are less than the statistical errors on the lifetimes.

C. $8P_{3/2}$ lifetime

We accumulate $8P_{3/2}$ lifetime data for periods of 1000 seconds with about 10^4 atoms in the trap, the probe laser on resonance, and with a 420 nm interference filter in the imaging system which directs the fluorescence onto the PMT. We repeat the counting measurement without atoms and obtain a flat background. The sloping background present in the 9s

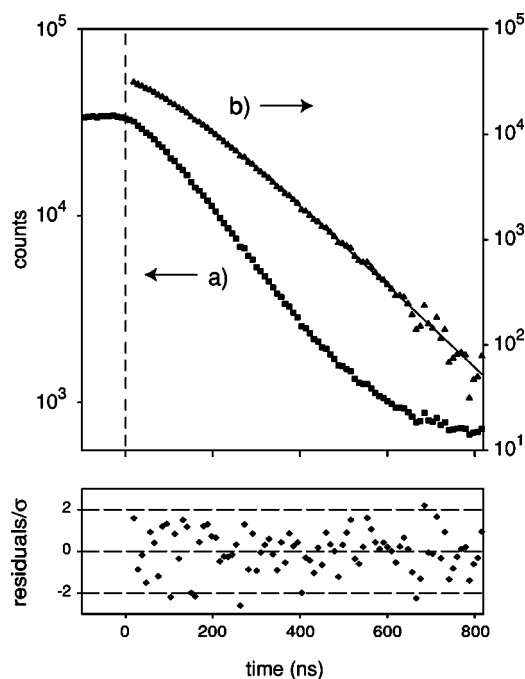


FIG. 10. Decay curve of the $8P_{3/2}$ level with fit residuals. (a) Binned data taken with a 420 nm interference filter. (b) Binned counts minus the background. The line is a fit of the data including the expected contamination from $8P_{1/2}$ photons. The lower plot shows the residuals of the fit divided by the statistical uncertainty of each point.

lifetime measurement is not detectable, since the difference in wavelengths is larger than before by almost a factor of two.

Since the $9S_{1/2}$ and $8P_{3/2}$ populations do not have time to stabilize before the excitation is turned off, we cannot use the exponential amplitudes given in Eq. (7). However, the atomic populations are close to steady state, and so we use the amplitudes of Eq. (7) as starting parameters for the fit. We fit the data (see Fig. 10) with the procedure outlined in the previous section (Sec. IV B) and obtain $\chi^2_{\nu}=0.96$.

I. Systematic errors

Since we measure the $8P_{3/2}$ lifetime with the same technique as the $9S_{1/2}$ lifetime, the two measurements have many sources of systematic errors in common. However, the differences in fitting procedure also introduce new sources of systematic errors. We take into account the following systematic errors in our error budget of the $8P_{3/2}$ lifetime.

(a) *TAC and MCA nonlinearity.* We calibrate the timing of the $8P_{3/2}$ pulse detection apparatus in the same manner as the for $9S_{1/2}$ measurement. While the technique is the same, the apparatus is physically distinct, and consequently shows some difference in performance. We measure the linear time calibration of the TAC and MCA with an uncertainty of $\pm 0.02\%$. The time scale has a nonlinearity, which adds an uncertainty of $\pm 0.13\%$ to the lifetime of the fitted data. We find that the height scale of the TAC and MCA taken together varies by roughly 1% over 1000 channels. This nonuniformity in the height scale influences the fitted lifetime by less than 0.13%.

(b) *Pulse pileup correction.* We keep this correction small by maintaining count rates of about one event every 50 cycles. The correction to the data provided by Eq. (2) affects the fitted lifetime of our data by less than 0.07%.

(c) *Truncation error.* We find that varying the start and end points of the data set does not lead to statistically significant changes in the fitted lifetime.

(d) *Quantum beats.* We populate the energy eigenstates of the $8p$ levels incoherently from the decay of the $9s$ level through the spontaneous emission of a photon. The loss of coherence between energy eigenstates during spontaneous emission eliminates the possibility of quantum beats in the decay of the $8p$ levels. The error due to variations in the filling rate of the $8P_{3/2}$ level from quantum beats in the decay of the $9s$ level are automatically included in the Bayesian error (see below) due to uncertainty in the $9s$ lifetime.

(e) *Contamination shift.* We find a contamination shift of $\delta\tau_2 = -0.10 \pm 0.04$ ns. The shift is much smaller than the statistical error on τ_2 .

(f) *Bayesian error.* Since we do not extract the $9s$ lifetime, τ_1 , from fits of the $8p$ data, the uncertainty in τ_1 affects the precision with which τ_2 can be extracted in a fit of the data. This source of uncertainty is Bayesian, since it is conditioned on our knowledge of τ_1 . τ_1 and τ_2 are not independent variables. The probability that the $8P_{3/2}$ lifetime is given by τ'_2 is

$$P(\tau'_2) = \int P(\tau'_1, \tau'_2) d\tau'_1 = \int P(\tau'_2 | \tau'_1) P(\tau'_1) d\tau'_1 \\ = \frac{1}{\sqrt{2\pi}\sigma_1} \int P(\tau'_2 | \tau'_1) \exp\left(-\frac{1}{2} \frac{(\tau'_1 - \tau_1)^2}{\sigma_1^2}\right) d\tau'_1, \quad (13)$$

where $\tau_1 = 107.53$ ns and $\sigma_1 = 0.90$ ns is the uncertainty in τ_1 . We determine the uncertainty in τ_2 due to the uncertainty in τ_1 , $P(\tau'_2 | \tau'_1)$, by fitting the data with several values of τ_1 . We find from the fits that the dependence of τ'_2 on τ'_1 is given to lowest order over the range $\tau'_1 = \tau_1 \pm 3\sigma_1$ by the following linear relation:

$$\tau_2(\tau'_1) = \tau_2 + \alpha(\tau'_1 - \tau_1), \quad (14)$$

where $\tau_1 = 107.53$ ns and $\tau_2 = 83.5$ ns, and empirically for our data we find $\alpha = -1.34$. The fitting error in τ_2 varies negligibly, so that we can describe $P(\tau'_2 | \tau_1)$ with the Gaussian probability distribution

$$P(\tau'_2 | \tau_1) = \frac{1}{\sqrt{2\pi}\sigma_2} \exp\left(-\frac{1}{2} \frac{[\tau'_2 - \tau_2(\tau_1)]^2}{\sigma_2^2}\right), \quad (15)$$

with $\tau_2(\tau_1)$ given by Eq. (14). The probability of having lifetimes τ'_1 and τ'_2 , $P(\tau'_1, \tau'_2)$, is plotted in Fig. 11. Upon integrating Eq. (13), we find that the Bayesian error is given by $\alpha\sigma_1 = \pm 1.20$ ns and adds in quadrature with σ_2 , the statistical error on τ_2 obtained from the fit.

(g) *Other systematic effects.* The density of the atoms in the trap is low ($\sim 10^9/\text{cm}^3$). In this regime, effects such as radiation trapping, superfluorescence, and quenching due to collisions do not alter the measured lifetime.

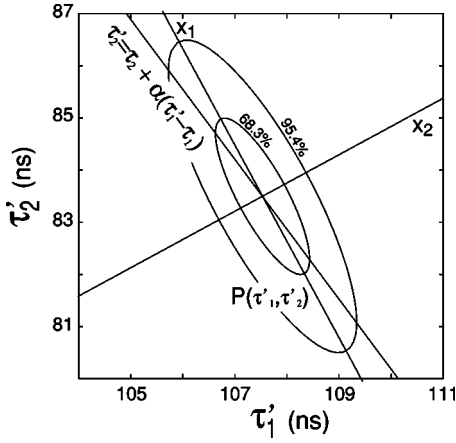


FIG. 11. Probability distribution plot of the $9s$ and $8P_{3/2}$ lifetimes, τ_1 and τ_2 . The percentages indicate boundaries of the 68.3% and 95.4% confidence level regions for $P(\tau'_1, \tau'_2)$. Note that the principal axes of the Gaussian distribution do not coincide with the linear relation for $\tau'_2(\tau'_1)$ of Eq. (14).

2. Summary of measurement

Table II contains the error budget for the lifetime measurements. The Bayesian error and to a lesser extent the statistics dominate the uncertainty in the measurement. Collecting photon counts for longer periods will not significantly reduce the error on the $8P_{3/2}$ lifetime, unless it leads to a reduced error on the $9s$ lifetime. Combining the uncertainties in quadrature gives a total uncertainty of $\pm 1.8\%$. We obtain a lifetime of 83.5 ± 1.5 ns for the $8P_{3/2}$ level of francium.

3. Comparison with theory

Figure 12 compares the $8P_{3/2}$ lifetime measurement with *ab initio* and semiempirical theoretical predictions. The $8P_{3/2}$ level decays to the $8s$, $7s$, and $6d$ levels. The matrix elements to these levels must be properly evaluated to predict the lifetime with Eqs. (3) and (4). The *ab initio* calculations of radial matrix elements of Safronova *et al.* [16] and Dzuba *et al.* [24] agree with the measured lifetime to better than one standard deviation. The agreement between theory and experiment provides confidence in the calculated values at large electronic radius of the $8P_{3/2}$ wave function. The agreement also gives confidence in the accuracy of the wave functions of the $7s$ and $8s$ levels, the main decay channels of the $8P_{3/2}$ level.

TABLE II. Error budget for the $8P_{3/2}$ lifetime measurement.

Error	$8P_{3/2}$ (%)
Statistical	± 1.05
Bayesian	± 1.44
TAC/MCA calibration	$< \pm 0.02$
TAC/MCA nonlinearity	± 0.13
TAC/MCA nonuniformity	± 0.13
Contamination shift error	± 0.05
Total	$\pm 1.8\%$

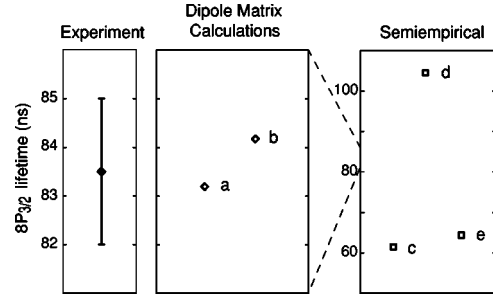


FIG. 12. Comparison of the measured $8P_{3/2}$ level lifetime with theoretical predictions from radial matrix elements (a) [16], (b) [17], and semiempirical calculations (c) [20], (d) [21], (e) [22].

D. $8P_{1/2}$ lifetime

1. Data and fits

We measure the $8P_{1/2}$ lifetime following the procedure of the $8P_{3/2}$ lifetime measurement. We accumulate $8P_{1/2}$ lifetime data with a 436 nm interference filter in the imaging system. Figure 13 shows an example of the data. We fit the data with the procedure used for the $8P_{3/2}$ lifetime and outlined in Sec. IV B, and obtain $\chi^2_\nu = 1.01 \pm 0.06$ over two data sets. The 436 nm filter has a transmission of 10% at the $8P_{1/2}$ decay wavelength of 433 nm, and consequently the photon count rate is much lower than with the 420 nm filter. We increase the transmission of the 433 nm filter by tilting it roughly 15° . While the tilt has the effect of sliding the band-pass of the filter to the blue and increasing the transmission at 433 nm, it also increases the transmission at 423 nm. In practice, the transmission at 423 nm is sufficiently large that the amplitude of the unwanted $8P_{3/2}$ counts must be included explicitly in a fit to the data. For the data taken with the tilted

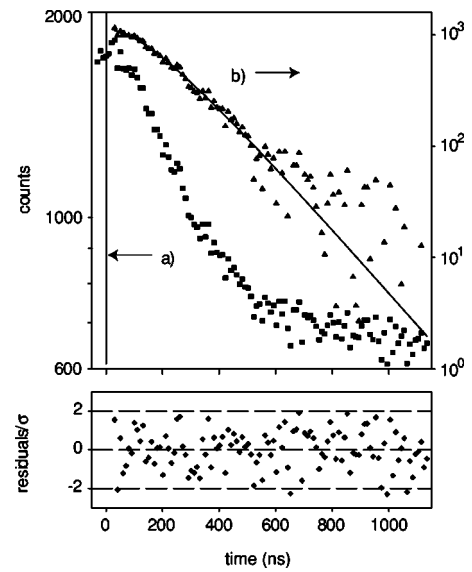


FIG. 13. Decay curve of the $8P_{1/2}$ level with fit residuals. (a) Binned data taken with 436 nm interference filter. (b) Binned counts minus the background. The line is a fit of the data including the expected contamination from $8P_{3/2}$ photons. The lower plot shows the residuals of the fit divided by the statistical uncertainty of each point.

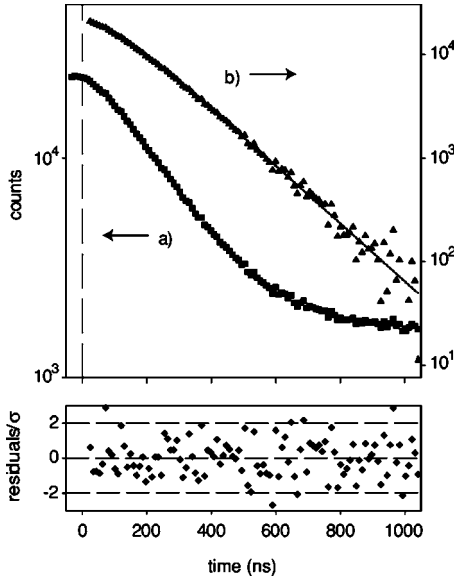


FIG. 14. Decay curve of the $8P_{1/2}$ level with fit residuals. (a) Binned data taken with a tilted 436 nm interference filter. (b) Binned counts minus the background. The line is a fit of the data. The lower plot shows the residuals of the fit divided by the statistical uncertainty of each point.

436 nm filter, we use Eq. (9) for the fit, which is equivalent to fitting to three exponential decays. We use $\tau_1 = 107.53$ ns, $\tau_2 = 83.5$ ns, and A_2/B_2 as fixed parameters, while varying the exponential amplitudes (C_2 , C_3 , and A_3/B_3), the $8P_{1/2}$ lifetime τ_3 , and the background b to optimize the fit. Figure 14 shows data taken with a tilted 436 nm filter and the corresponding fit. While tilting the filter increases the counting rate, the additional counts from 423 nm photons significantly limit the precision with which τ_3 can be extracted from the data. We obtain a comparable uncertainty on τ_3 with the tilted filter as we do with a nontilted filter. With this method, we obtain $\chi^2_{\nu} = 0.99 \pm 0.02$ over several data sets.

2. Systematic errors

Since we measure the $8P_{1/2}$ lifetime with the same technique as the $8P_{3/2}$ lifetime, the two measurements have the same sources of systematic errors. We do not find a truncation error in our fits, the measurement is not subject to quantum beats, and the density of atoms in the trap is too low for effects such as trapping, superfluorescence, and quenching due to collisions to affect the measured lifetime. We include the following systematic errors in our error budget of the $8P_{1/2}$ lifetime.

(a) *TAC and MCA nonlinearity.* We measure the linear time calibration of the TAC and MCA with an uncertainty of $\pm 0.04\%$. The time scale has a nonlinearity, which adds an uncertainty of $\pm 0.065\%$ to the lifetime of the fitted data. We find that the height scale of the TAC and MCA taken together varies by roughly 1% over 1000 channels. This nonuniformity in the height scale influences the fitted lifetime by less than 0.23%.

(b) *Pulse pileup correction.* We keep this correction

TABLE III. Error budget for the $8P_{1/2}$ lifetime measurement.

Error	$8P_{1/2}$ (%)
Statistical	± 2.30
Bayesian	± 0.44
TAC/MCA calibration	$< \pm 0.04$
TAC/MCA nonlinearity	± 0.07
TAC/MCA nonuniformity	± 0.23
Contamination shift error (untilted data only)	± 0.6
Total	$\pm 2.4\%$

small by maintaining low count rates of about one event every 400 cycles. The correction to the data given by Eq. (2) affects the fitted lifetime of our data by less than 0.14%.

(c) *Contamination shift.* For the data taken with an untilted 436 nm filter, we find an average contamination shift of $\delta\tau_3 = +1.65 \pm 0.90$ ns. The shift is smaller than the statistical error on τ_3 . There is no contamination shift for the data taken with the tilted 436 nm filter, since the the amplitude of the unwanted 423 nm counts is obtained directly from the fits.

(d) *Bayesian error.* We derive τ_3 from fits in which we use $\tau_1 = 107.53 \pm 0.90$ ns and $\tau_2 = 83.5 \pm 1.5$ ns as fixed parameters. We must account for how the uncertainties in τ_1 and τ_2 influence the uncertainty in τ_3 . We follow the method developed earlier for the Bayesian error on τ_2 due to τ_1 . The generalization of the method to two parameters must include the fact that τ_1 and τ_2 are not independent parameters. The problem is simplified considerably by the symmetry of the probability distribution $P(\tau_1, \tau_2)$, represented in Fig. 11. We note that in a coordinate system (x_1, x_2) rotated to match the major and minor axes of $P(\tau_1, \tau_2)$, the probabilistic variables x_1 and x_2 are independent. The probability of obtaining τ_3 as the lifetime of the $8P_{1/2}$ level is given by

$$\begin{aligned}
 P(\tau_3) &= \int P(\tau'_1, \tau'_2, \tau'_3) d\tau'_1 d\tau'_2 = \int P(x'_1, x'_2, \tau_3) dx'_1 dx'_2 \\
 &= \int P(\tau_3 | x'_1, x'_2) P(x'_1, x'_2) dx'_1 dx'_2 \\
 &= \int P(\tau_3 | x'_1) P(x'_1) dx'_1 \int P(\tau_3 | x'_2) P(x'_2) dx'_2, \quad (16)
 \end{aligned}$$

where we have used the fact that the Jacobian of the change of variable $(\tau_1, \tau_2) \rightarrow (x_1, x_2)$ is unity, since a rotation conserves surface area. We determine $P(\tau_3 | x_1)$ and $P(\tau_3 | x_2)$ empirically by fitting the $8P_{1/2}$ data with different values of x_1 and x_2 . The tilted and untilted interference filter data are fit simultaneously with a global χ^2 , which is the sum of the individual χ^2 for each data set. Each data set is fit with the appropriate fitting function, but with τ_3 as a shared free parameter, while the exponential amplitudes remain independent. The statistical error on τ_3 varies negligibly for fits over the ranges of $-2\sigma_{x_1} \leq x_1 \leq +2\sigma_{x_1}$ and $-2\sigma_{x_2} \leq x_2 \leq +2\sigma_{x_2}$, so that we can consider it constant. $P(\tau_3 | x_1)$ and $P(\tau_3 | x_2)$ are both Gaussian in nature, and consequently all errors add in

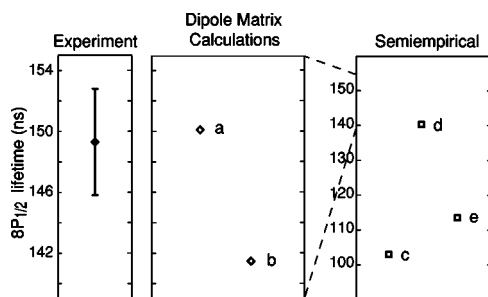


FIG. 15. Comparison of the measured $8P_{3/2}$ level lifetime with theoretical predictions from radial matrix elements (a) [16], (b) [24], and semiempirical calculations (c) [20], (d) [21], (e) [22].

quadrature. We find that the uncertainty in τ_3 due to the uncertainty in x_1 is 0.65 ns, and the uncertainty in τ_3 due to the uncertainty in x_2 is 0.13 ns. The total Bayesian error on τ_3 due to uncertainties in τ_1 and τ_2 is 0.66 ns.

3. Summary of measurement

Table III contains the combined error budget for the lifetime measurements obtained with both the tilted and untilted interference filter. The statistics dominate the uncertainty of the measurement. Adding the uncertainties in quadrature gives a total uncertainty of $\pm 2.4\%$. We obtain a lifetime of 149.3 ± 3.5 ns for the $8P_{1/2}$ level of francium.

4. Comparison with theory

We compare the $8P_{1/2}$ lifetime measurement with both *ab initio* and semiempirical theoretical predictions in Fig. 15. The $8P_{1/2}$ level decays to the $8s$, $7s$, and $6D_{3/2}$ levels. The lifetime is determined by inserting the calculated matrix elements to these levels into Eq. (3) and Eq. (4). The *ab initio*

calculation of radial matrix elements of Safronova *et al.* [16] agrees well with the measured lifetime to better than the experimental error. The matrix elements of Dzuba *et al.* [24] predict the measured lifetime to within -2.5σ .

V. CONCLUSION

The measurements of the $9s$, $8P_{3/2}$, and $8P_{1/2}$ lifetimes show good agreement with the theoretical predictions based on *ab initio* MBPT calculations of the radial matrix elements involved in the radiative decay of the three levels. In the case of the $9s$ and $8P_{3/2}$ levels, the agreement demonstrates the accuracy of these calculations, and provides a basis for confidence in the wavefunctions calculated by Safronova *et al.* [16] and Dzuba *et al.* [24] at large electronic radii. For the $8P_{1/2}$ levels the agreement between theory and experiment is not within the experimental error, and so our numbers provide a challenge to the calculations involved in the decay of the $8P_{1/2}$ level. The accuracy of the measurement of the lifetime of the $9s$ level is better than a percent, while for the $8p$ levels the accuracy is around 2%. The generally good agreement between measurement and theory provides further confidence that an atomic parity nonconservation measurement should allow for the accurate extraction of standard model parameters.

ACKNOWLEDGMENTS

This work has been supported by the NSF. E.G. acknowledges support from CONACYT. The authors thank K. Gulyuz, B. Gutshow, R. Lefferts, and J. Sell for the operation of the Stony Brook LINAC, and Professor J. Marecek for the use of the CARY 1 UV-Visible spectrometer.

-
- [1] J. E. Simsarian, S. Aubin, J. S. Grossman, L. A. Orozco, M. R. Pearson, G. D. Sprouse, and W. Z. Zhao, in *Parity Violations in Atoms and Polarized Electron Scattering*, edited by Bernard Frois and Marie-Anne Bouchiat (World Scientific, Singapore, 1999), p. 312.
- [2] E. Gomez, S. Aubin, L. A. Orozco, G. D. Sprouse, and D. DeMille (unpublished).
- [3] M.-A. Bouchiat and C. Bouchiat, *Rep. Prog. Phys.* **60**, 1351 (1997).
- [4] I. B. Khriplovich, *Parity Non-Conservation in Atomic Phenomena* (Gordon and Breach, New York, 1991).
- [5] V. V. Flambaum and D. W. Murray, *Phys. Rev. C* **56**, 1641 (1997).
- [6] E. Gomez, S. Aubin, L. A. Orozco, and G. D. Sprouse (unpublished).
- [7] S. Aubin, E. Gomez, L. A. Orozco, and G. D. Sprouse, *Rev. Sci. Instrum.* **74**, 4342 (2003).
- [8] D. V. O'Connor and D. Phillips, *Time Correlated Single Photon Counting* (Academic, London, 1984).
- [9] L. Young, W. T. Hill III, S. J. Sibener, S. D. Price, C. E. Tanner, C. E. Wieman, and S. R. Leone, *Phys. Rev. A* **50**, 2174 (1994).
- [10] B. Hoeling, J. R. Yeh, T. Takekoshi, and R. J. Knize, *Opt. Lett.* **21**, 74 (1996).
- [11] R. G. DeVoe and R. G. Brewer, *Opt. Lett.* **19**, 1891 (1994).
- [12] J. E. Simsarian, L. A. Orozco, G. D. Sprouse, and W. Z. Zhao, *Phys. Rev. A* **57**, 2448 (1998).
- [13] J. M. Grossman, R. P. Filler III, L. A. Orozco, M. R. Pearson, and G. D. Sprouse, *Phys. Rev. A* **62**, 062502 (2000).
- [14] S. Aubin, E. Gomez, L. A. Orozco, and G. D. Sprouse, *Opt. Lett.* **28**, 2055 (2003).
- [15] W. Z. Zhao, J. E. Simsarian, L. A. Orozco, and G. D. Sprouse, *Rev. Sci. Instrum.* **69**, 3737 (1998).
- [16] M. S. Safronova, W. R. Johnson, and A. Derevianko, *Phys. Rev. A* **60**, 4476 (1999); M. Safronova (personal communication).
- [17] V. A. Dzuba and V. V. Flambaum (personal communication).
- [18] M. Marinescu, D. Vranceanu, and H. R. Sadeghpour, *Phys. Rev. A* **58**, R4259 (1998).
- [19] J. E. Simsarian, W. Shi, L. A. Orozco, G. D. Sprouse, and W. Z. Shao, *Opt. Lett.* **21**, 1939 (1996).
- [20] W. A. van Wijngaarden and J. Xia, *J. Quant. Spectrosc. Radiat.*

- Transf. **61**, 557 (1999).
- [21] E. Biémont, P. Quinet, and V. Van Renterghem, J. Phys. B **31**, 5301 (1998).
- [22] C. E. Theodosiou, Bull. Am. Phys. Soc. **39**, 1210 (1994); personal communication.
- [23] C. J. Bowers, D. Budker, E. D. Commins, D. DeMille, S. J. Freedman, A.-T. Nguyen, S.-Q. Shang, and M. Zolotarev, Phys. Rev. A **53**, 3103 (1996).
- [24] V. A. Dzuba, V. V. Flambaum, and J. S. M. Ginges, Phys. Rev. A **63**, 062101 (2001).